Direct synthesis and characterization of high quality tin oxide nanopowders by in-flight oxidation of flame

P. KATHIRVEL[*]
GRD Centre for Materials Research, Department of Physics, PSG College of Technology, Coimbatore-641004, Tamilnadu, India

Highly crystalline Tin oxide (SnO_2) nanoparticles were directly synthesized from inexpensive metallic tin (Sn) powder by flame synthesis technique. The rapid melting and oxidation of Sn in a high temperature oxidative flame produce the crystalline and pure SnO_2 nanoparticles, as evident from X-ray Diffraction (XRD) and Field Emission Scanning Electron Microscopy (FESEM) analysis. The residence time and oxidation time was calculated using basic fluid dynamics equations. The particle size calculated by XRD analysis found to be 24 nm. The good stoichiometry of SnO_2 nanoparticles were supported by Energy Dispersive X-ray Analysis (EDAX). The band gap of the SnO_2 nanoparticles was calculated using Kubelka-Munk function and found to be 3.4 eV.

1. Introduction

Preparing nanoparticles with uniform morphology is prime issue in the field of nanoscience and technology. Metal oxides play a key role as active materials for solar cells due to their unique combination of optical, electrical and charge transport properties [1]. Metals are able to form a large diversity of oxide compounds. In technological applications, oxides are used in the fabrication of microelectronic circuits, sensors, piezoelectric devices, fuel cells, anti corrosion coatings and as catalysts [2-4]. In nanotechnology, the goal is to prepare nanostructures with special properties compared to the bulk materials. Enormous efforts are being directed towards the development of nanometer sized metal oxides in order to understand their fundamental mechanisms such as size effect, quantum effect for the practical applications of these materials. Particle sizes in the nano regime and specific crystal morphologies are expected to enhance the performance and allow the fine tuning of the properties of these materials. Among the other metal oxides tin oxide creates interest because it is a naturally non- stoichiometric prototype transparent conducting oxide (TCO) [5]. It has high transparency in visible region and high reflectivity in IR region. Structural and optical properties of tin oxide are of great importance from the technological point of view [6]. One of the most important methods to modify the characteristics of the materials is the method of preparation. A number of processing methods such as co-precipitation, sol-gel, spray pyrolysis and hydrothermal method [7-10] have been developed for the preparation of SnO_2 nanoparticles.

The principle of flame synthesis is the melting and oxidation of molten metal powders in a flame, thereby forming stable metal oxide followed by nucleation and agglomeration. Compared to the other synthesis methods this is one of the suitable methods of metal oxide nanoparticles synthesis because the product can be formed directly in one step and the desired phase can also be achieved because of the high temperature of the flame. Flame synthesis is an easy synthesis method where the product properties can be tuned by changing the composition of the precursor gas and the flame operating conditions.

The present work reports the preparation of phase pure SnO_2 nanoparticles by in-flight oxidation of flame synthesis and its structural, optical and surface morphological properties.

2. Experimental details

Flame synthesis is a process of utilizing the heat of the flame. The nozzle mixes fuel gas acetylene with oxygen in the $50O_2$:$50C_2H_2$ ratio. The tin (Sn) metal powder of average particle size approximately 40 μm was fed into the flame by gravitational feed and Sn metal powder melts in the oxy-acetylene flame and reacts with oxygen which results the formation of tin oxide (SnO_2) nanoparticles as shown in the Fig. 1. It was collected from the powder collector and used for further characterization.
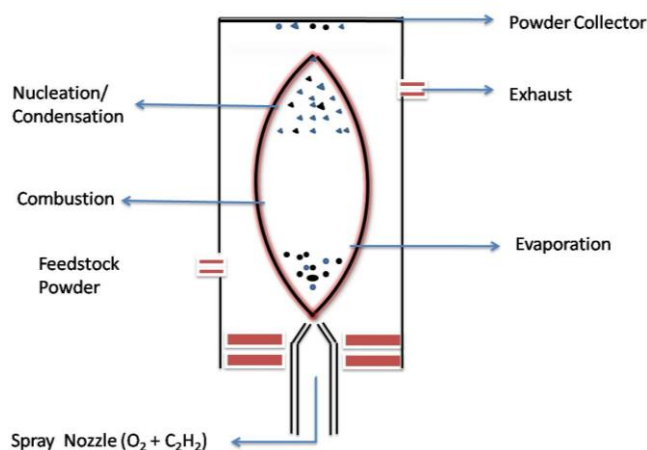
Fig. 1. Schematic diagram of flame oxidation

Fig. 2. XRD pattern of SnO₂ nanoparticles

3. Characterization

The synthesized SnO₂ nanoparticles were characterized for their structural, surface morphological, compositional analysis and optical properties. Optical transparency in the visible region and characteristic absorption in the UV region of SnO₂ nanoparticles in solution were measured by using UV-Visible spectrophotometer (Shimadzu, model no. 1650). XRD (Bruker D8 Advance) was subjected to characterize phase purity, shape, nanocrytalline structure and average crystalline size calculated using Debye-Scherrer relation and the diffraction pattern was recorded at 2θ :20°-90° using a CuKα1 radiation with λ=1.5460Å. The analysis of morphology (size and shape) was traced out by conducting Scanning Electron Microscopy, SEM (Hitachi, model no. 33400).

4. Results and discussion

X –Ray diffraction

Fig. 2 depicts typical X-ray diffraction pattern of SnO₂ nanoparticles formed by in-flight oxidation of flame synthesis. All the diffraction peaks are indexed as tetragonal structure with lattice constants a=4.74 Å and c=3.19 Å in accordance with the values in the standard JCPDS pattern file no. 01-070-6153. It is further observed that there is no indication of secondary phase which evinces the phase purity of the flame synthesized nanoparticles and conversion of feedstock metallic Sn into SnO₂ in the flame. The average particle size (D) is determined by using the Scherer formula [11].

$$D = \frac{0.9\lambda}{\beta \cos\theta}$$

(1)

where D is the crystallite size, 0.9 is the shape factor, λ is the X-ray wavelength (Cu K_α-1.54Å), β is the full width at half maximum of the diffraction peak, and θ is the Bragg diffraction angle. The average particle size calculated is 24 nm.

Elemental composition

The chemical composition of SnO₂ nanoparticles is confirmed from the energy dispersive X-ray spectrum (EDAX) which is shown in Fig. 3. The EDAX analysis exhibits clear peaks of Sn and O elements and the atomic percentages of Sn and O elements present in the nanoparticles is 75.99 and 22.01 mass%, respectively which indicates that the prepared SnO₂ nanoparticles have very good stoichiometry.
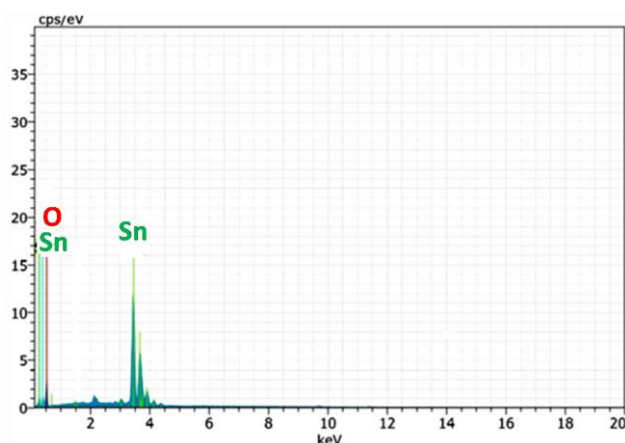
Fig. 3. EDAX Spectrum of SnO₂ nanoparticles

In order to choose the appropriate size of the feedstock (Sn metal powder), for effective conversion of metal into metal oxide, the effect of feedstock size on the oxidation of the same was estimated using basic fluid

dynamics and combustion equations. The residence time (T_{res}) of metallic Sn powder in the oxidative flame was estimated from the thermo-physical properties of the flame and feedstock using the following equation [12]

$$T_{res} = \left(\frac{2S}{kV_g}\right)^{1/2}$$

(2)

where k is the constant and V_g is the gas velocity. The oxidation time (T_{oxi}) of the metal powder inside the flame was calculated from diffusion coefficient (z) of oxygen into the flame, size (d_p), density (ρ_p) of the feedstock and density (ρ_g) of flame forming gas using the following equation [13]

$$T_{oxi} = \frac{\rho_p \, d_p^2}{8 \, \rho_g \, Z \ln 2.12}$$

(3)
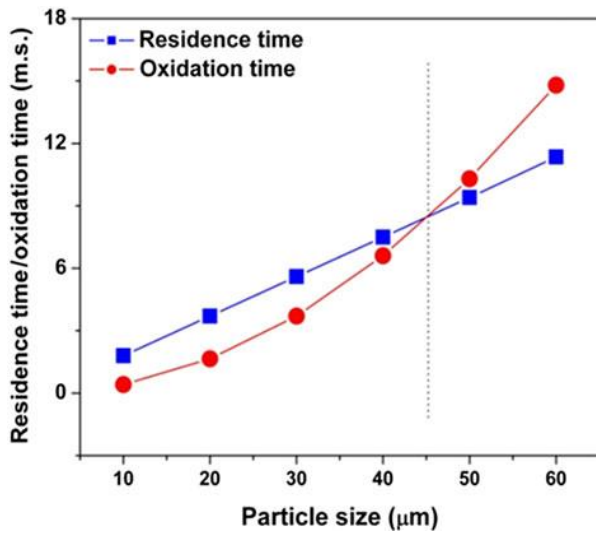
Fig. 4. Oxidation time of different size Sn powders in oxy-acetylene flame

Fig. 4 shows the residence and oxidation time of feedstock metallic Sn powders in the flame. It is noted that the resident time increases with increase in powder size whereas the oxidation time exponentially varies and intercepts at around 45 μm size of the feedstock powders. It means that the maximum size of the feedstock powder should be 45 μm otherwise the product SnO$_2$ nanoparticles will have unmelted Sn or unoxidized metallic powders.

Optical studies

To determine the band gap of synthesized SnO$_2$ nanoparticles, the reflectance spectrum of SnO$_2$ nanoparticles prepared by flame synthesis technique is

measured. The reflectance (R) Spectrum of the SnO$_2$ nanoparticles is shown in Fig. 5.

Absorbance spectrum of the flame synthesized SnO$_2$ nanoparticles is shown in Fig. 6. It is observed that a strong absorption band starts at 320 nm and edge at 350 nm. The absorption of higher photon energy (greater than bandgap energy) excites an electron from the valence band to conduction band which is an essential requirement in charge transport mechanism in solar cells.
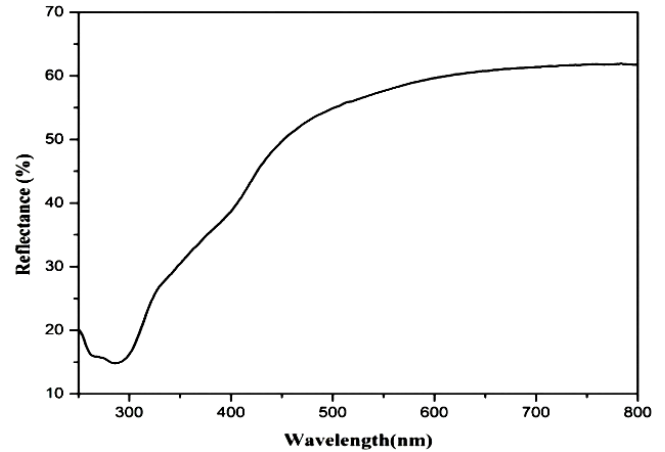
Fig. 5. Reflectance Spectrum of SnO$_2$ nanoparticles
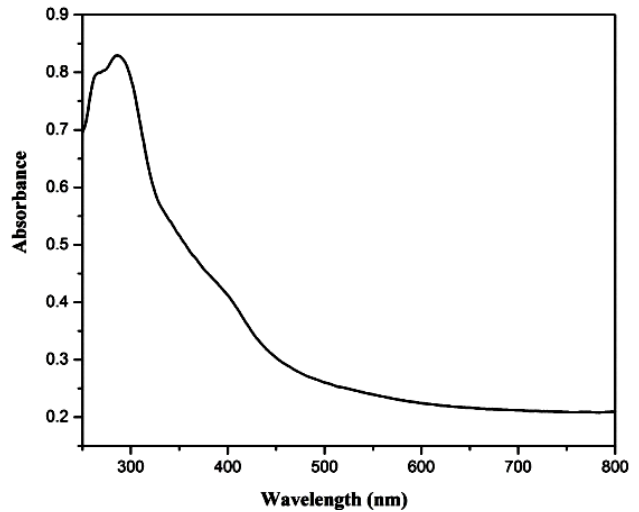
Fig. 6. Absorbance Spectrum of SnO$_2$ nanoparticles

In order to determine the precise value of optical band gap of the SnO$_2$ nanoparticles, the reflectance values are converted to absorbance by Kubelka-Munk function [14]. The Kubelka- Munk theory is generally used for the analysis of diffuse reflectance spectra obtained from weak absorbing samples.

$$f(R) = \frac{(1 - R)^2}{2R}$$

(4)

where, f(R) is the Kubelka-Munk function which corresponds to the absorbance, R is the reflectance. It is well known that the optical transitions in tin oxide are direct transition. The absorption coefficient a for direct transitions is calculated by the following relation [15]

$$(\alpha h\upsilon) = A(h\upsilon - E_g) \quad (5)$$

where α is the linear absorption coefficient of the material, A is an energy-independent constant and E_g is the band gap. The f(R) values for the SnO_2 nanoparticles are obtained using the equation 4. Considering the Kubelka–Munk scattering coefficient as constant with respect to wavelength, and using the Eq. (4) we shall obtain the expression

$$(f(R)h\upsilon)^2 = A(h\upsilon - E_g) \quad (6)$$
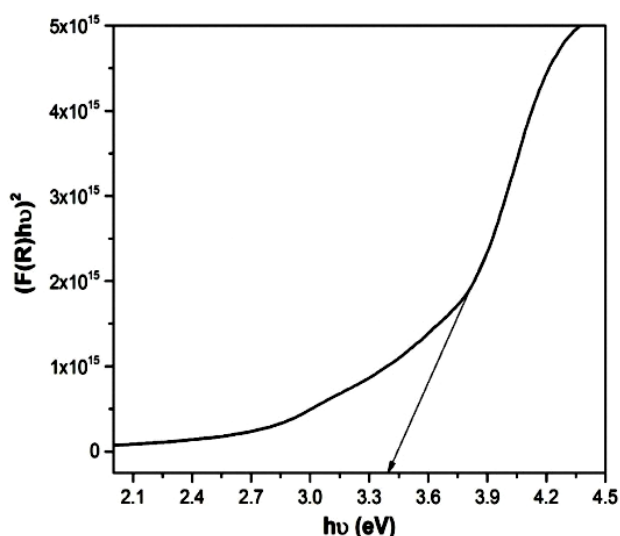
Fig. 7. Bandgap of SnO₂ nanoparticles

Therefore, F(R) values are obtained from equation 3. The curve of $(f(R)h\upsilon)^2$ Vs.$h\upsilon$ for the SnO_2 nanoparticles is plotted, as shown in Fig. 7. The band gap (E_g) of SnO_2 nanoparticles is determined from curve of $(f(R)h\upsilon)^2$ vs. $h\upsilon$ and found to be 3.4 eV.

Surface morphology analysis

Scanning electron microscopy is one of the powerful tools to study the surface morphology of the nanostructures at the atomic level. The surface morphology of the feedstock metallic tin (Sn) powders is shown in Fig. 8. The secondary electrons scattered from the metallic Sn powder were detected to trace the image. It is noticed that irregular morphology and different size of about 40 μm with a fairly non uniform distribution. Large Size agglomeration/grains are noticed which is due to joining of similar size particles having almost same surface area and surface energy.
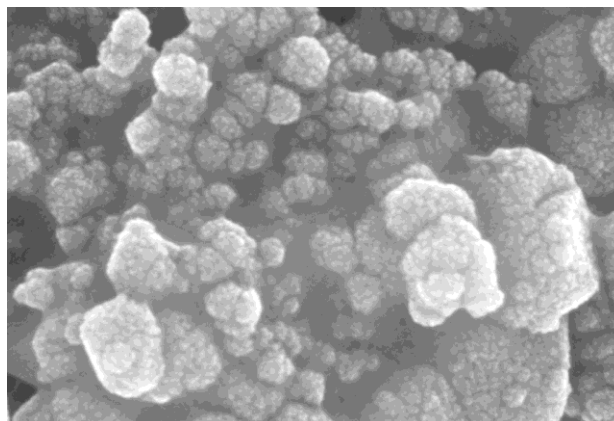
Fig. 8. SEM micrograph of feedstock metallic tin (Sn) powders

The FESEM image of the flame synthesized tin oxide nanoparticles is shown in Fig. 9. It is clear that the different size of the particles of the feedstock metallic Sn powders (Melting point of Sn is 453K) initially melts at the surface level which dissociates the agglomerations into individual particles   and later starts melting completely at the core of the flame as the temperature of the flame at the core is around 2300K. It is also noticed that the melted Sn powders react with oxygen in turn forms vertically grown SnO_2 homogeneous nanosheet like structure which are supported by XRD studies without any secondary phases in the nanopowders.
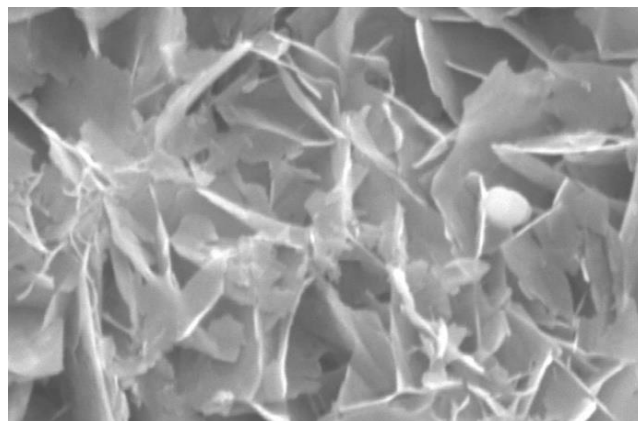
Fig. 9. FESEM micrograph of flame oxidized tin oxide (SnO₂) nanoparticles

5. Conclusion

SnO_2 nanopowders have been successfully prepared from the commercial tin metal powder by a simple in flight oxidation of flame synthesis technique. The structural, optical and morphological properties of SnO_2 nanoparticles were studied. XRD spectrum indicates that the prepared SnO_2 nanoparticles are highly crystalline and phase pure in nature. The particle size of the SnO_2

nanoparticles, estimated from XRD using Scherer formula is 24 nm. The bandgap of the SnO_2 nanoparticles is found to be 3.4 eV. The FESEM confirms the nanosheet like structure formation of SnO_2 nanoparticles. Since the morphology of the flame synthesized SnO_2 is homogeneous and has good absorption coefficient it can be used a charge transport layer in solar cells and light emitting diodes.

References

[1] G. Faglia et al., Appl. Phy. Lett. **86**, 11923 (2005).
[2] Brion Bob et al., Chem. of Mat. **25**, 4725 (2013).
[3] Y. Wang et al., J. Phys. Chem. B **10**, 817 (2004).
[4] H. Sugimoto et al., Eur. J. Chem. **23**, 4550 (2004).
[5] J. S. Lee et al., J. Cryst. Growth **267**, 145 (2004).

[6] K. Bouras et al., J. Mater. Chem. C **2**, 8235 (2015).
[7] A. Chandra Bose et al., J. Phys. Chem. Solids **64**, 659 (2003).
[8] Deliang Chen et al., Chem. Phys. Lett. **398**, 201 (2004).
[9] R. R. Kasar et al., Physica B: Cond. Mat. **403**, 3724 (2008).
[10] Dipyaman Mohanta et al., RSC Adv. **6**, 110996 (2016).
[11] P. Kathirvel et al., J. Alloys and Compds **590**, 341 (2014).
[12] S. Kumar et al., Comput. Mat. Sci. **36**, 451 (2006).
[13] A. M. Kanury, Introduction to Combustion Phenomena, Gordon and Beach Science Publishers, New York, 86 (1975).
[14] H. Snaith et al., Phys. Rev. B **74**, 045306 (2006).
[15] W. Tress et al., Adv. Ener. Mat. **5**, 1400812 (2015).

_____
[*]Corresponding author: ponkathirvel@gmail.com